Lasers in Surgery and Medicine 26:432–440 (2000)

Preliminary Study of In Vivo Autofluorescence of Nasopharyngeal Carcinoma and Normal Tissue

Jianan Y. Qu, PhD,[1]* Po Wing, MD,[2] Zhijian Huang, PhD,[1] Dora Kwong, MD,[3] Jonathan Sham, MD,[3] Siu Lung Lee, MS,[1] Wai Kuen Ho, MD,[2] and William I. Wei, MD[2]

[1]Department of Electrical and Electronic Engineering, Hong Kong University of Science and Technology, Clear Water Bay, Kowloon, Hong Kong, People's Republic of China
[2]Division of Otorhinolaryngology, The University of Hong Kong, Queen Mary Hospital, The University of Hong Kong, Hong Kong, People's Republic of China
[3]Department of Clinical Oncology, The University of Hong Kong, Hong Kong, People's Republic of China

Background and Objective: **In nasopharyngeal cancer, conventional white light endoscopy does not provide adequate information to detect the flat/small lesion and identify the margin of observable tumor. In the present study, we evaluate the potential of light-induced fluorescence spectroscopic imaging for the localization of cancerous nasopharyngeal tissue.**
Study Design/Materials and Methods: **We built a multiple channel spectrometer specifically for the investigation of fluorescence collected by a conventional endoscopic system. Nasopharyngeal fluorescence were measured in vivo from 27 subjects during the routine endoscopy. The biopsy specimens for histologic analysis were taken from the tissue sites where the fluorescence were measured.**
Results: **Two algorithms to discriminate the nasopharyngeal carcinoma from normal tissue were created based on the good correlation between the tissue autofluorescence and histologic diagnosis. For the two-wavelength algorithm, carcinoma can be differentiated from normal tissue with a sensitivity and specificity of 93% and 92%, respectively. For the three-wavelength algorithm with compensation of variation of blood content in tissue, a sensitivity of 98% and specificity of 95% were achieved.**
Conclusion: **Fluorescence endoscopic imaging used with the algorithms developed in this report is an efficient method for detecting the nasopharyngeal carcinoma. Lasers Surg. Med. 26:432–440, 2000.**

Key words: LIF spectroscopy; endoscopy; in vivo diagnosis; nasopharyngeal cancer

INTRODUCTION

Nasopharyngeal carcinoma (NPC) occurs with highest incidence and frequencies in Asian countries. Genetic factors, infection with the Epstein-Barr virus (EBV), and environmental factors are all implicated as being important for the development of NPC [1–4]. Screening of nasopharyngeal carcinoma is now carried out by checking individuals suspected of having NPC for elevated levels of serum IgA antibodies directed against EBV viral capsid antigen (VCA) and early antigen (EA) with subsequent nasoendoscopic biopsy of the nasopharynx. However, many malignant tumors and early lesions such as carcinoma in situ

Contract grant sponsor: Hong Kong Research Grants Council; Contract grant number: CA97/98.EG01; Contract grant number: HKUST6207/98P; Contract grant sponsor: Hong Kong University of Science and Technology.

*Correspondence to: Jianan Y. Qu, PhD, Department of Electrical and Electronic Engineering, Hong Kong University of Science and Technology, Clear Water Bay, Kowloon, Hong Kong. E-mail: eequ@ust.hk

Accepted 15 December 1999

are small and have a flat surface. It is difficult to localize the small and flat lesions with an ordinary endoscopy. Random biopsies are usually conducted to screen for subclinical tumors. According to the statistic results, only 5.4% of patients with elevated serum EBV antibody titer had asymptomatic NPC in random biopsy of the nasopharynx [3]. The low incidence of pathologic evidence of nasopharyngeal carcinoma suggests that majority of the screening program will suffer the unnecessary trauma caused by the random biopsy. Furthermore, patients with raised serum EBV antibody titer or with tumor removed need to have follow-up endoscopy and biopsy to rule out possible nasopharyngeal carcinoma, residual tumor, or tumor recurrence. As a result, a remote imaging technique is desirable for early detection of malignant tumor and guiding the routine biopsy procedure.

It has been shown that the optical characteristics of tissue, such as absorption, scattering, and fluorescence provide the valuable diagnostic information regarding tissue biochemical composition and pathologic state. In particular, many groups have explored the use of light-induce fluorescence (LIF) spectroscopy by means of optical fiber catheter and endoscopic imaging system for noninvasive detection of diseased tissue on many human organ sites. A comprehensive review of characterization of tissue by LIF spectroscopy has been given by Wagnieres et al. [5]. The promising results show that the spectral characteristics of endogenous tissue fluorescence (autofluorescence) induced by low-power excitation source can partially reveal the physiochemical composition and morphology of the tissue. Thus, LIF spectroscopic technique may have the potential to discriminate the nasopharyngeal carcinoma from the surrounding normal tissue.

Human tissue is a kind of turbid medium. Light is absorbed and highly scattered during the propagation in tissue. The measurement and interpretation of the LIF spectra recorded on the tissue surface become complicated because the intrinsic LIF signal is modulated by the optical properties of tissue. It has been shown that the LIF spectral characteristics are dependent on the excitation and collection geometry such as illumination area and uniformity, incident, and collection angles [6–12]. The use of the multiple optical fiber catheter to collect LIF signal from tissue in vivo successfully eliminated the geometrical effects on the fluorescence measurement [6,8,9]. The catheter is gently contacted to the tissue surface during the signal collection. The excitation and collection geometry is fixed with the design of the distal tip of the catheter and independent of the measurement site. Various algorithms were successfully applied to characterize tissue based on the in vivo LIF spectra collected by the optical fiber catheter [6,13,14]. This approach has achieved high sensitivity and specificity to diagnose the diseased tissue. However, the point-by-point measurement is time consuming, especially for examination of a large area of tissue. Clinically, an imaging method is more desirable. Several groups have developed the LIF imaging system for early detection of malignant tumors based on the difference in fluorescence spectral characteristics between diseased and normal tissue [15–18].

The excitation and collection geometry for a LIF imaging system is more complicated than the optical fiber catheter-based approach. Instead of fixed geometry, the detector-tissue separation and incident/collection angle vary in a wide range across the imaged tissue surface because of the large area illumination and irregularity of the tissue surface. It is more challenging to create a reliable algorithm to discriminate the diseased tissue from normal tissue for a fluorescence imaging system. In this work, we built a multiple-channel spectrometer for the study of characteristics of in vivo fluorescence signal recorded by an imaging system. Specifically, the spectrometry analyzed the LIF signal of tissue in the image plane of a conventional endoscopic system during endoscopy. This method allowed us to investigate the fluorescence signal received by each pixel of a two-dimensional sensor proposed for recording the LIF image of the fluorescence endoscopy. First, we created a simple algorithm to detect nasopharyngeal carcinoma by using the ratio of fluorescence signals at two wavelength bands. Furthermore, we tested the algorithm involved with the fluorescence signals at three wavelength bands to compensate for the effect of blood absorption on the fluorescence signal. The performance of the algorithm should be more stable with reducing the distortion of tissue fluorescence signal by the variation of blood content. Finally, we discuss the possibility to further improve the sensitivity and specificity of the LIF imaging technique. Instead of using a general algorithm built on the spectral data collected from a group of subjects, we propose to make use of the difference of fluorescence signals between diseased and normal tissue within an individual to create a more ro-

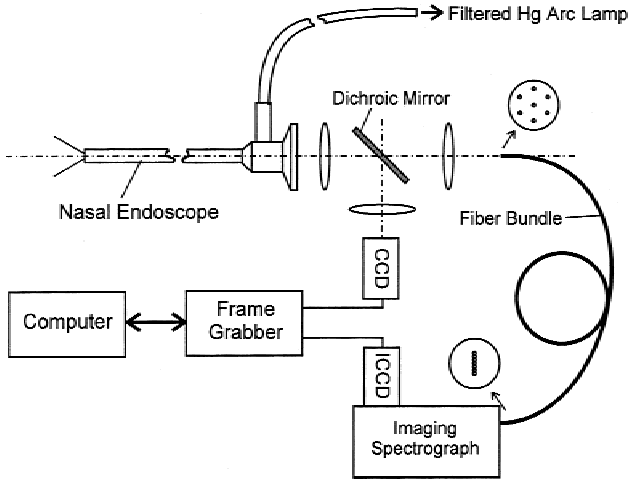

Fig. 1. Arrangements for in vivo measuring tissue autofluorescence in the image plane of a nasal endoscopic imaging system. CCD, charge coupled device camera; ICCD, intensified CCD camera.

bust algorithm for the detection of diseased tissue.

METHODS AND MATERIALS

The schematic of the system for collection of in vivo fluorescence signal is shown in Figure 1. The system was designed to study the fluorescence signal recorded in the excitation and collection geometry of any endoscope. A 100 W mercury arc lamp (Oriel Instruments Model 60100) filtered by a band pass filter (Omega Optical Inc. 420DF60) in the wavelength range from 390–450 nm was used as excitation source. The excitation power at the endoscope tip is approximately 50 mW. The fluorescence and reflection of excitation from the tissue surface were imaged by a commercial endoscope (Karl Storz 7200A). A dichroic mirror with cut-on wavelength at 470 nm (Omega Optical Inc. 470DRLP) divided the optical signal from the endoscope into the reflection and fluorescence channels. The image recorded by a CCD video camera in reflection channel was displayed on a monitor for the real time endoscopy. A long pass filter (Omega Optical Inc. 470EELP) with cut-off wavelength at 470 nm was used to eliminate residual excitation light in the fluorescence channel. The fluorescence signal was collected by an optical fiber bundle with seven optical fibers of 200 μm in diameter and NA 0.16. The fibers were evenly distributed in fluorescence image plane of the endoscope. When the separation of the endoscope distal tip and the imaged tissue surface was

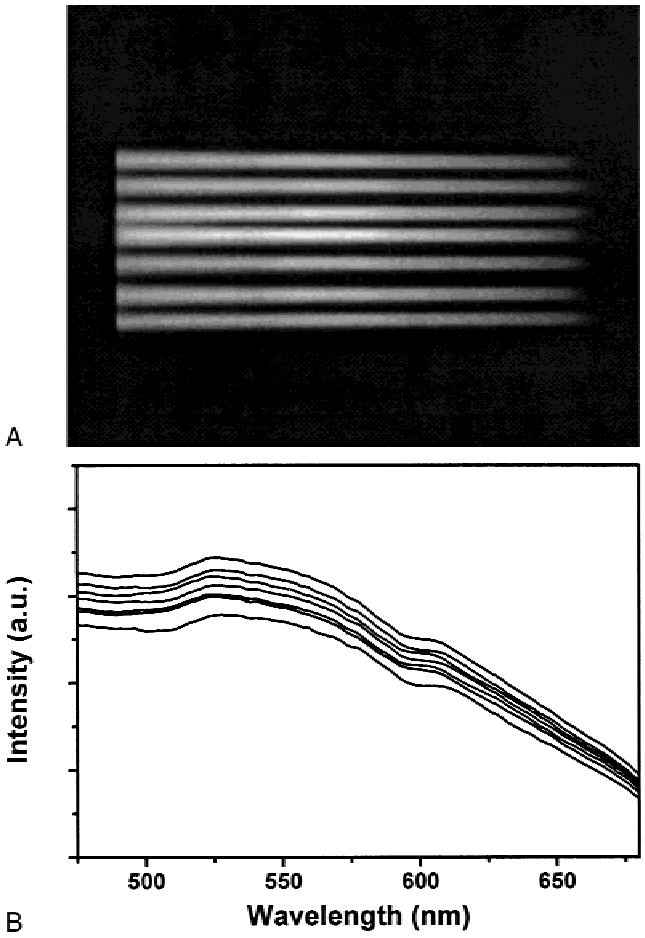

Fig. 2. **A:** Spectrally dispersed images of optical fibers recorded by intensified charge coupled device camera from a white light source. **B:** Spectra formed by binning the spectral strips vertically.

15 mm, each single fiber sampled the signal from the area approximately 1 mm in diameter on tissue surface. The sampling area is much smaller than the total illuminated area. The fluorescence signals received by the fibers were conducted to the entrance slit of an imaging spectrograph (Oriel Instruments Model 77480). The tips of optical fibers were placed in the entrance plane and lined up vertically. The fluorescence conducted by the fibers were then dispersed and imaged onto an intensified CCD (ICCD) camera (CID Technologies, Inc. ICID3712DX3). The images of CCD and ICCD were grabbed simultaneously by a frame grabber (Matrox Genesis-LC) at rate of 25 frames per second. A typical spectral image recorded by the ICCD camera is shown in Figure 2A. The spectra of a white light lamp shown in Figure 2B were formed by binning the seven spectral strips in the image vertically. The wavelength

of the spectral measurement was calibrated by using a standard spectral lamp (Ocean Optics Inc. HG-1). The response of ICCD with fixed gain was in its linear region.

It is important to guide the clinician to precisely select the tissue site for fluorescence measurement and performing biopsy. Aiming the area of interest for measurement of tissue fluorescence was determined with the marks in the real time video image displayed on the monitor. The marks indicated the sampling areas of seven fibers. The calibration of aiming marks was conducted in two steps. First, optical fiber tips in the image plane of the endoscopic imaging system were illuminated by a white light source from the other ends connected to the spectrograph. The fiber tips in the image plane were then imaged on a white card placed approximately 15 mm away from the endoscope distal tip. Based on the reversibility law of light, the images of fiber tips were correspondent to the sampling areas of fibers. However, the images of fiber tips on the card could not be captured by the CCD because of wavelength selectivity of the dichroic mirror. We marked the sampling areas (fiber tip images) on the white card and made them visible for CCD. Next, the image with marked sampling areas was grabbed from CCD. The positions of the sampling areas were then marked in an image overlaid together with the real time reflection video image captured by the CCD camera. This method enabled the clinician to precisely point one of seven fibers nearest to the area of interest and take the fluorescence measurement during endoscopy. This design made the measurement convenient and flexible. A typical image grabbed from real time video with aiming marks is shown in Figure 3.

The in vivo fluorescence measurements have been conducted in the Department of Otorhinolaryngology and Department of Clinical Oncology at Queen Mary Hospital, The University of Hong Kong. A total of 27 subjects were enrolled in this study, which lasted approximately 6 months. The fluorescence spectra were measured at the sites where biopsy specimens were taken. Histologic examinations on biopsies were then performed by the pathologists. This study was approved by the Ethical Committee of Queen Mary Hospital, the University of Hong Kong.

RESULTS AND DISCUSSION

From 27 subjects, 110 biopsy specimens were collected during in vivo fluorescence measurement procedure, in which, 58 were found to be normal, 52 exhibited carcinoma. Figure 4 illustrates typical fluorescence spectra acquired from nasopharyngeal sites in three subjects. All fluorescence intensities are not calibrated because of variation of measurement geometry site by site. As can be seen, the spectral lineshapes vary not only individual by individual but within individual also. The peak emission wavelength of nasopharyngeal carcinoma and normal tissue occurs within ±10 nm of 510 nm. The large variation of fluorescence intensity in the region of 530–590 nm and peak emission wavelength indicates that the blood content in tissue plays important role in the distortion of fluorescence signal recorded on the tissue surface [11,12,19,20]. During the fluorescence measurement procedure, the distance between the distal tip of endoscope and tissue surface was kept in the range from 10 to 15 mm. Although the distance was not calibrated, we observed that the fluorescence intensity from the nasopharyngeal carcinoma was generally lower than the normal tissue.

A simple algorithm based on the ratio of fluorescence signals at two wavelength bands was created to differentiate the nasopharyngeal carcinoma from the surrounding normal tissue. As discussed previously, the algorithm will be valid for the fluorescence endoscopic imaging system because the tissue fluorescence were analyzed in the image plane of the endoscope. A set of wavelength

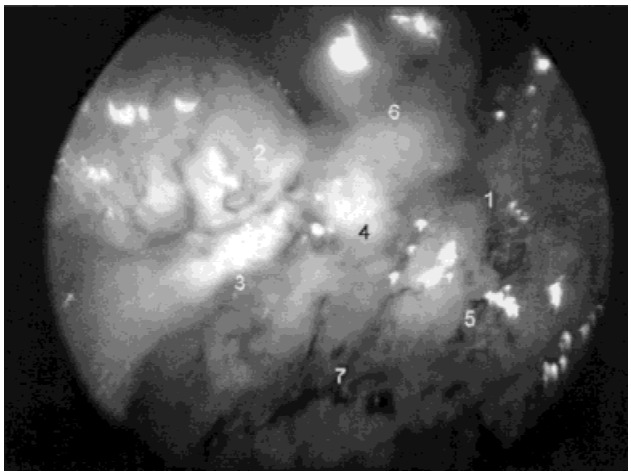

Fig. 3. Real time image recorded from the endoscope overlaid with aiming number marks of seven optical fibers. Each mark indicates the area aimed by a correspondent single fiber. Fluorescence signals are collected from seven sampling areas simultaneously. The highlighted number points the area of interest on the tissue surface where both fluorescence measurement and biopsy will be taken.

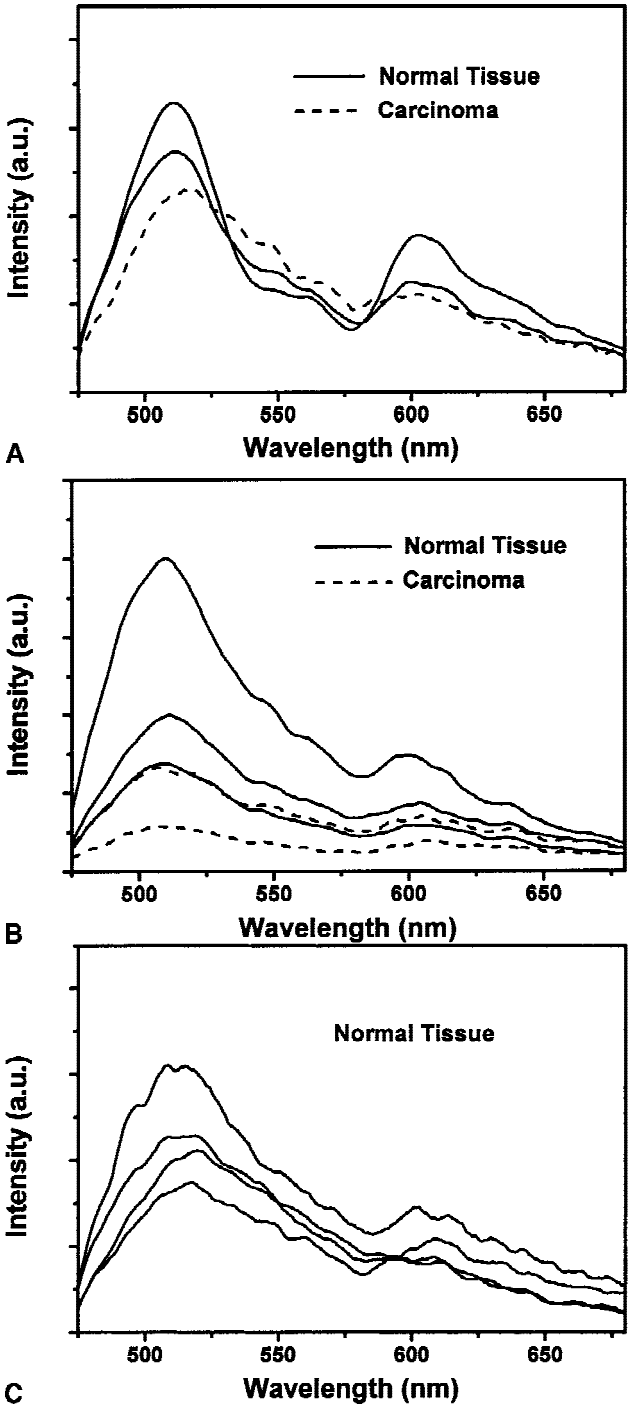

Fig. 4. **A–C:** Typical in vivo autofluorescence emission spectra collected from different sites of three subjects.

bands in the range from 470–700 that best separated the carcinoma and normal tissue was found by exhaustive search. The minimal bandwidth was set to 30 nm in the search. A very narrow bandwidth becomes not practical because the signal to noise ratio SNR is inversely proportional to

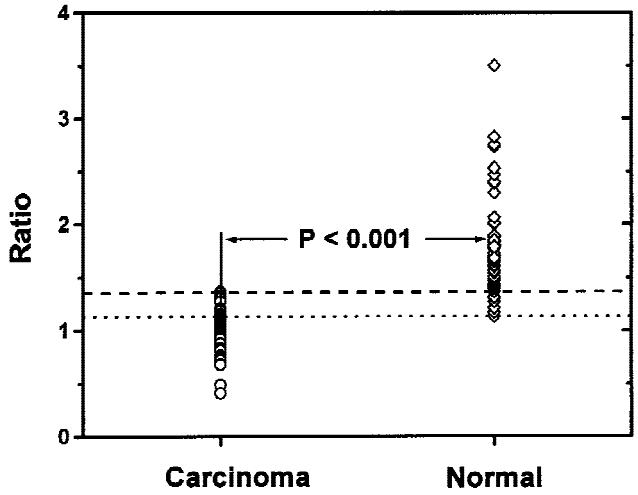

Fig. 5. Scatter plot for the scores of the two-wavelength ratio algorithm. The circles and diamonds represent the scores of nasopharyngeal carcinoma and normal tissue, respectively.

the bandwidth and the performance of a fluorescence imaging system is strongly dependent on the SNR. The ratio of fluorescence signal in the short wavelength band vs. long wavelength band was calculated. An unpaired Student's t-test was used to compare the ratio scores of the normal and carcinoma tissues. The separation of normal tissue from carcinoma was evaluated by the Student's t-test result. The optimal wavelength bands for the ratio algorithm was found at 500 ± 25 nm and 640 ± 40 nm. The ratio of the signals in the band of 500±25 nm vs. 640±40 nm from all measured fluorescence spectra are shown in Figure 5. The distributions of the ratio scores for normal and carcinoma are displayed separately because of the slight overlapping between two groups. The mean ratio scores were 1.78 ± 0.48 for normal nasopharyngeal tissue and 0.99 ± 0.20 for the carcinoma. The P-value of Student's t-test on the ratios for normal tissue and carcinoma was found to be smaller than 0.001. This value indicates the significantly statistical difference ($P < 0.001$) between two groups of scores. To further evaluate the performance of two-wavelength algorithm, we calculated the sensitivity and specificity of the algorithm as a function of decision thresholds. The sensitivity and specificity were defined as

$$Sensitivity = \frac{True\ Positives}{True\ Positives + False\ Negatives}$$

$$Specificity = \frac{True\ Negatives}{True\ Negatives + False\ Positives}.$$

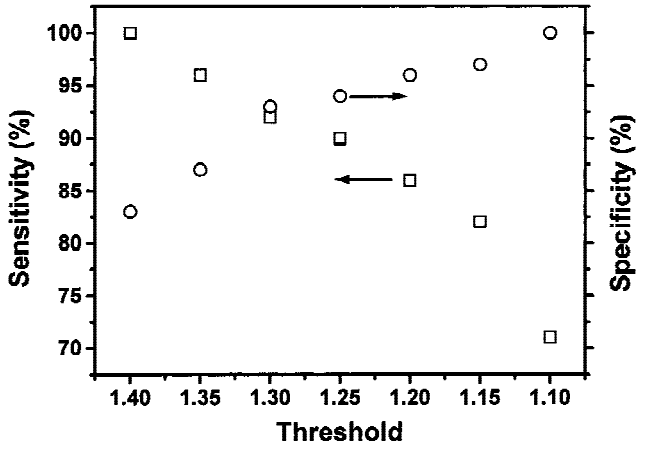

Fig. 6. Dependence of sensitivity and specificity of the two-wavelength algorithm on the diagnostic threshold. The squares and circles represent sensitivity and specificity, respectively.

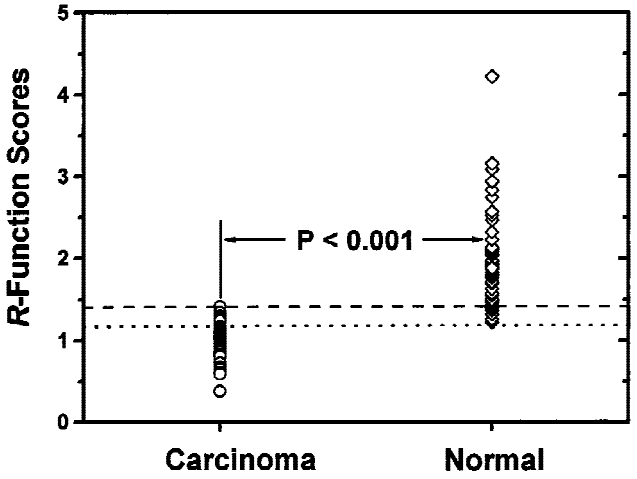

Fig. 7. Scatter plot for the scores of the three-wavelength *R*-function algorithm. The circles and diamonds represent the scores of nasopharyngeal carcinoma and normal tissue, respectively.

The dash and dot lines in Figure 5 represent the diagnostic thresholds for sensitivity of 100% and specificity of 100%, respectively. The dependence of sensitivity and specificity on diagnostic threshold are shown in Figure 6. As can be seen, when the threshold is set to 1.30, the two-wavelength algorithm can achieve both sensitivity and specificity approximately 92%.

As discussed in the beginning of the section, the variation of blood content plays an important role in distortion of fluorescence spectra emitted from tissue surface. The result of an exhaustive search of the optimal set of wavelength bands for the ratio algorithm has reflected the effect of blood content on the fluorescence measurement. The optimal set of wavelength bands at 500 ± 25 nm and 640 ± 40 nm excludes the wavelength region of 530 to 590 nm where the blood appears to have very strong absorption [19,20]. This finding indicates that the exhaustive search is a process to minimize the blood effect on the performance of the ratio algorithm. However, the absorption coefficient of blood in the wavelength band of 500 ± 25 nm is still much greater than 640 ± 40 nm [19,20]. To further reduce the effect of blood absorption and improve the accuracy of the diagnosis, we investigated an algorithm that compensated the variation of fluorescence signal in wavelength band of 500 ± 25 nm caused by blood absorption to some extent.

The algorithm was created by forming the dimensionless function

$$R = \frac{I(500 \pm 25)}{I(640 \pm 40)}\left(\frac{I(500 \pm 25)}{I(560 \pm 35)}\right)^{k}$$

in which fluorescence signals in three wavelength bands: 500 ± 25 nm, 560 ± 35 nm, and 640 ± 40 nm were used. The first term of *R*-function is the two-wavelength ratio. The second term includes the information of blood absorption and is used to compensate the effect of blood variation on the first term. A constant k was used to scale the blood effect on the score of the algorithm. It has been found in an exhaustive search that the best separation was achieved by setting the value of k approximately 0.51. Again, the result of an unpaired student's *t*-test was used as the criterion to determine the best separation and optimal value of constant k. The scores of *R*-function for normal and carcinoma tissues are shown in Figure 7. The mean scores of *R*-function for normal and carcinoma tissues are 1.95 ± 0.50 and 1.00 ± 0.21, respectively. The small P value (< 0.001) demonstrates that the significantly statistical difference between two groups of scores. It has been noticed that the variances of *R*-function scores for normal and carcinoma tissues are at the same levels as the two-wavelength algorithm. However, the difference of mean score between the normal tissue and carcinoma is 0.95, compared with 0.79 of two-wavelength algorithm. This finding indicates that three-wavelength algorithm can separate the normal tissue and carcinoma better than two-wavelength algorithm. The dependence of sensitivity and specificity on the diagnostic threshold for three-wavelength algorithm is displayed in Figure 8. The sensitivity of 98% and specificity of 95% can be achieved when the threshold is set to 1.35.

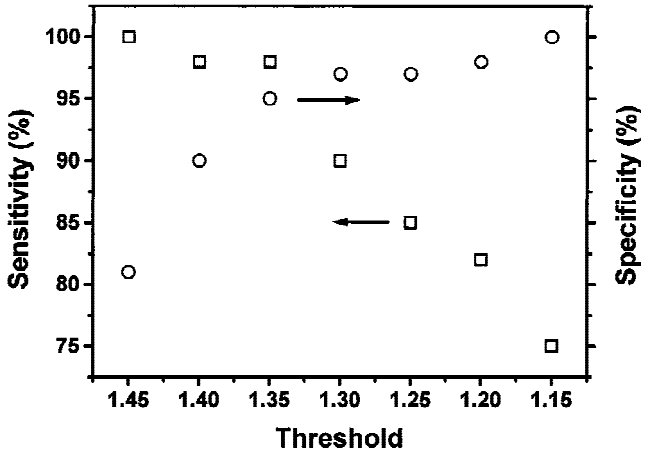

Fig. 8. Dependence of sensitivity and specificity of the three-wavelength *R*-function algorithm on the diagnostic threshold. The squares and circles represent sensitivity and specificity, respectively.

The biopsy specimens from 15 of the total 27 subjects enrolled in this study exhibited both normal and carcinoma tissues. Because the fluorescence measurements were performed at the same sites where the biopsies were taken, we can compare the scores of two- and three-wavelength algorithms for normal and carcinoma tissues back to back within an individual from these 15 subjects. The results are shown in Figure 9A,B. The numbers of normal and carcinoma biopsy specimens from the 15 subjects are 36 and 26, respectively. The difference in mean scores between normal and carcinoma tissues for each subject are calculated and displayed in Figure 10. The separation of carcinoma from normal tissue is obviously improved by compensating the blood absorption with the three-wavelength algorithm. It is an interesting finding that the score of carcinoma is always lower than normal tissue within an individual, although it is not generally true that score of normal tissue is always higher than carcinoma individual by individual. This finding suggests that the score contrast in an image taken from an individual may be used to differentiate normal tissue from carcinoma. The image can be created by the use of two-wavelength ratio algorithm or three-wavelength *R*-function algorithm. One may take the advantage of widely applied pattern-recognition technique, for example the edge detection algorithm to detect the score contrast in an image and localize the diseased tissue [21]. However, it should be noticed that in this study the fluorescence spectra were collected from various sites point by point within an individual. The characteristics of fluorescence spectra are

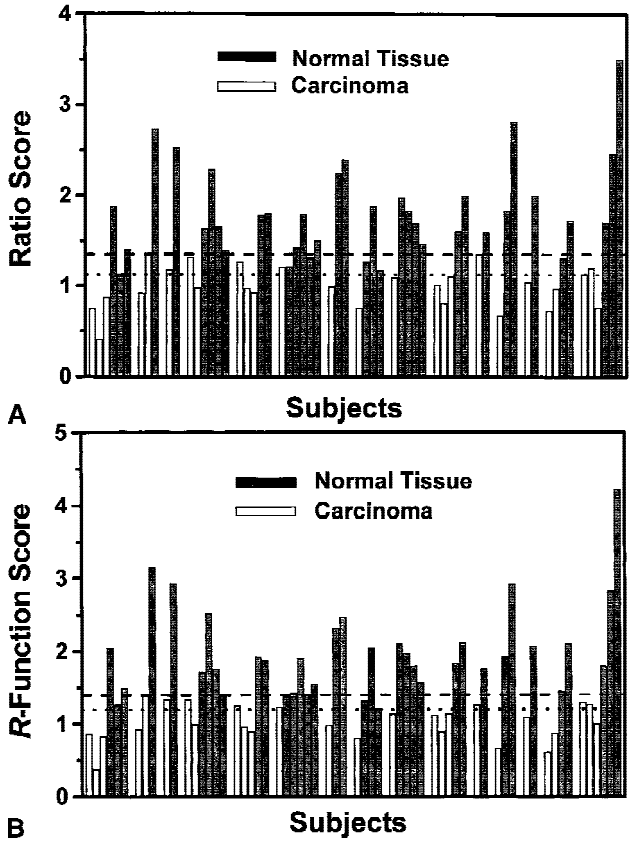

Fig. 9. Back to back comparison of scores for nasopharyngeal carcinoma and normal tissue within the individual and individual by individual. **A:** Two-wavelength ratio algorithm. **B:** Three-wavelength *R*-function algorithm.

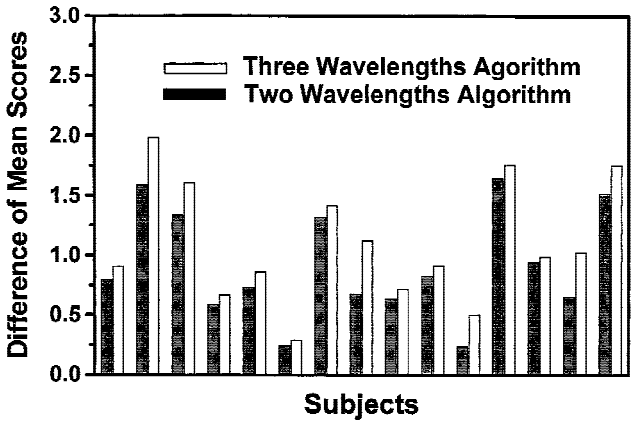

Fig. 10. Difference between mean score of carcinoma and mean score of normal tissue for two- and three-wavelength algorithms within the individual.

modulated by a variety of geometrical factors, such as homogeneity of illumination and excitation/emission angles. The fluorescence excitation and collection geometry are different from site by site. Therefore, the scores of normal and carci-

noma tissue vary in a fairly wide range, because the fluorescence measurement was performed at different sites. To develop a reliable pattern-recognition algorithm, the fluorescence signals must be collected from the diseased tissue and connected normal tissue in the surrounding area. This approach will at least ensure that the fluorescence of lesion and its surrounding normal tissue near the boundary are measured in the same excitation and collection geometry. The fluorescence signals recorded in this study are not suitable to create a pattern recognition algorithm such as the edge detection, because the measurement sites were usually not close to each other.

Although the score of normal tissue may vary in a wide range over the whole imaged tissue because of the geometrical effect, the score contrast between the normal tissue in the adjacent area should be small except for drastic variations of tissue surface. To further explore the approach of score contrast imaging, a spectral imaging system incorporated with two-wavelength ratio or three-wavelength R-function algorithm is needed to map the score over the tissue surface. Much more score data will be available to build the algorithm of pattern recognition. The correlation between the pathologic state of imaged tissue and its relative score over the whole ratio or R-function image then can be used to create a reliable algorithm. Based on our observation that score of carcinoma is always lower than normal tissue within an individual, the proposed score contrast imaging method may be more robust than two- and three-wavelength algorithms built on the fluorescence spectra collected from a group of subjects.

CONCLUSIONS

We built a multiple channel spectrometer to analyze the light induced fluorescence spectra of nasopharyngeal carcinoma and normal tissue in the image plane of a standard nasal endoscope. The results of the study reported here demonstrate that a conventional endoscopic system with the feature of fluorescence spectral imaging can localize the nasopharyngeal carcinoma with high sensitivity and specificity. There is not a technical obstacle and cost problem to build a two-wavelength and three-wavelength imaging system for real time endoscopy [15–18]. The fluorescence endoscopy will offer unique information for the early detection of malignant nasopharyngeal tumors noninvasively. The method to investigate the tissue autofluorescence in our study can be generally used to create reliable algorithm for various fluorescence endoscopic imaging systems to detect diseased tissue on other organ sites. It should be pointed out that no subject with a subclinical cancerous lesion was found and examined in this 6 months pilot study. The pathologic analysis showed that all biopsied sites, where the in vivo fluorescence spectra were measured, exhibited either normal or invasive carcinoma, although some carcinoma lesions are flat and unobservable. Furthermore, the exact biochemical and morphologic basis for the difference in fluorescence spectral characteristics between healthy and carcinoma tissue are currently unknown. In the future study, we will focus on investigating the autofluorescence of early lesion and develop the understanding of the basis of nasopharyngeal autofluorescence.

REFERENCES

1. Ho JHC. Genetic and environmental factors in nasopharyngeal carcinoma. In: Nakahara W, et al, editors. Recent advances in human tumor virology and immunology. Tokyo: University of Tokyo Press; 1971. p 275–295.
2. Ho JHC, Ng MH, Kwan HC, Chau JCW. Epstein-Barr virus-specific IgA and IgG serum antibodies in nasopharyngeal carcinoma. Br J Cancer 1976;34:655–659.
3. Wei WI, Sham JS, Zong YS, Choy D, Ng MH. The efficacy of fiberoptic examination and biopsy in the detection of early nasopharyngeal carcinoma. Cancer 1991;67:3127–3130.
4. Sham JS, Wei WI, Kwan WH, Chan CW, Kwong WK, Choy D. Nasopharyngeal carcinoma. Pattern of tumor regression after radiotherapy. Cancer 1990;65:216–220.
5. Wagnieres GA, Star WM, Wilson BC. In vivo fluorescence spectroscopy and imaging for oncological applications. Photochem Photobiol 1998;68:603–632.
6. Cothren RM, Richards-Kortum R, Sivak MV Jr, Fitzmaurice M, Rava RP, Boyce GA, Doxtader M, Blackman R, Ivanc TB, Hayes GB, Doxtader M, Blackman R, Ivanc T, Feld MS, Petras RE. Gastrointestinal tissue diagnosis by laser-induced fluorescence spectroscopy at endoscopy. Gastrointest Endosc 1990;36:105–111.
7. Hung J, Lam S, LeRiche JC, Palcic B. Autofluorescence of normal and malignant bronchial tissue. Lasers Surg Med 1991;11:99–105.
8. Ramanujam N, Mitchell MF, Mahadevan A, Thomsen S, Silva E, Richards-Kortum R. Fluorescence spectroscopy: a diagnostic tool for cervical intraepithelial neoplasia (CIN). Gynecol Oncol 1994;52:31–38
9. Qu J, MacAulay C, Lam S, Palcic B. Laser-induced fluorescence spectroscopy at endoscopy: tissue optics, Monte Carlo modeling, and in vivo measurements. Opt Eng 1995;34:3334–3343.
10. Zeng HS, Weiss A, Cline R, MacAulay CE. Real time endoscopic fluorescence imaging for early cancer detection in the gastrointestinal tract. Bioimaging 1998;6:151–165.
11. Wu J, Feld MS, Rava RP. Analytical model for extracting

intrinsic fluorescence in turbid media. Appl Opt 1993;32: 3585–3595.
12. Gardner CM, Jacques SL, Welch AJ. Fluorescence spectroscopy of tissue: recovery of intrinsic fluorescence from measured fluorescence. Appl Opt 1996;35:1780–1792
13. Ramanujam N, Mitchell MF, Mahadevan A, Thomsen S, Malpica A, Wright T, Atkinson N, Richards-Kortum R. Development of a multivariate statistical algorithm to analyze human cervical tissue fluorescence spectra acquired in vivo. Lasers Surg Med 1996;19:46–62.
14. Tumer K, Ramanujam N, Ghosh J, Richards-Kortum R. Ensembles of radial basis function networks for spectroscopic detection of cervical precancer. IEEE Trans Biomed Eng 1998;45:953–961.
15. Andersson-Engels S, Johansson J, Svanberg K, Svanberg S. Fluorescence imaging and point measurements of tissue: applications to the demarcation of malignant tumors and atherosclerotic lesions from normal tissue. Photochem Photobiol 1991;53:807–814.
16. Palcic B, Lam S, Hung J, MacAulay C. Detection and localization of early lung cancer by imaging techniques. Chest 1991;99:742–743.
17. Andersson-Engels S, Johansson J, Svanberg S. Medical diagnostic system based on simultaneous multispectral fluorescence imaging. Appl Opt 1994;33:8022–8029.
18. Wagnieres GA, Studzinski AP, van den Bergh HE. An endoscopic fluorescence imaging system for simultaneous visual examination and photodetection of cancers. Rev Sci Instrum 1997:68:203–212.
19. van Kampen EJ, Zilstra WG. Determination of hemoglobin and its derivatives. In: H. Sobotka H, Stewart CP, editors. Advances in clinical chemistry, vol 8. New York: Academic; 1965. p 158–187.
20. van Assendelft OW. Spectrophotometry of haemoglobin derivatives. Netherlands: Royal Vangorcum Ltd; 1970. p 55–70.
21. Gonzalez RC, Woods RE. Digital imaging processing. New York: Addison-Wesley Publishing Co. Inc; 1993. p 413–477.